Scene Adaptive Building Individual Segmentation Based on Large-Scale Airborne LiDAR Point Clouds

Wangshan Yang, Yongjun Zhang, *Member, IEEE*, Xinyi Liu, and Boyong Gao

***Abstract*— Building individual segmentation plays a crucial role in building querying, management, analysis, and attribute addition. Previous research on this topic has primarily concentrated on small-scale scenes and single-type buildings. However, when dealing with complex scenes that contain diverse buildings, existing methods for building individual segmentation often encounter challenges, such as excessive undersegmentation and oversegmentation. To tackle this issue, we propose a scene adaptive building individual segmentation (SABIS) based on large-scale airborne LiDAR point clouds. The method first segments the roof object and then extract elevation feature and area feature of the roof object. Based on these features, the building point cloud is classified into two categories: urban scene buildings and rural residential scene buildings. Finally, for urban scene buildings, the building individual segmentation method based on the cylinder model consistency is used. For rural residential scene buildings, the building individual segmentation method based on bidirectional saliency features is employed. In this article, the proposed SABIS algorithm is quantitatively evaluated by using three large scene datasets at home and abroad and four benchmark methods. All kinds of accuracy are significantly better than the most advanced algorithms.**

***Index Terms*— Airborne LiDAR point clouds, building individual segmentation, building type classification, feature extraction, object segmentation.**

I. Introduction

THE 2019 Geomatics Developers Conference highlighted the need to shift from the traditional mapping approach based on scale classification to entity-based mapping. The concept of scale needs to be transformed from a multiscale database to a nonscale geospatial entity holographic database. During the 2020 Geomatics Technology Innovation Conference, Academician Liu Xianlin emphasized that the results of new mapping are structured, and the characteristic of new mapping is focused on entity level rather than map sheet-based mapping. The structured steps include hierarchical classification (semantic segmentation), object-oriented management (individual segmentation), and the generation of 3-D vector structures. The key aspect of knowledge production is to attach attributes to individual objects. Prof. Zhang Yongjun from Wuhan University highlighted in the 2022 Aerospace Vision Wisdom Lecture Hall and Geospatial Information Industry Conference that real-world 3-D is constructed by applying structured and semantic information to geospatial entities, enabling human–computer compatible understanding and real-time physical perception. The hierarchical division of real-world 3-D construction includes terrain-level models, urban-level models, and component-level models. Urban-level models mainly represent urban styles and terrain features within a specific area, with oblique photography models and individualized models being the mainstream forms. Individualization refers to the segmentation of classified data to obtain individualized 3-D model data.

In recent years, the rapid advancement of photogrammetry technology has made it possible to quickly acquire 3-D models of the Earth's surface. However, the current 3-D models represent the surface of the terrain as a whole, lacking the capability for individual querying, processing, and analysis of each object. This limitation hampers the wide-ranging application of 3-D models. To address this issue, a building segmentation method is employed to segment building point clouds into individual buildings. This segmentation allows for independent selection and assignment of attributes to each building, enabling building management, querying, analysis, and parallel reconstruction. Building individual segmentation plays a crucial role in point cloud-based building modeling. Presently, research on building individual segmentation primarily focuses on building scenes where the distance between buildings is significantly larger than the point cloud point spacing [1], as shown in Fig. 1(a). Only a limited number of studies have addressed cases where the spacing between buildings is comparable to the point cloud point spacing [2], as shown in Fig. 1(b). For complex building scenes and building point clouds with spatial arrangements similar to the point spacing, the task of separating adjacent buildings into individual building becomes challenging, as illustrated in Fig. 1(c) and (d). Failure to segment these buildings into individual building can have adverse effects on attribute addition, statistical queries, and building analysis. To fulfill the requirements of thematic querying, the reconstructed

Manuscript received 7 February 2024; revised 3 May 2024 and 22 June 2024; accepted 14 July 2024. Date of publication 17 July 2024; date of current version 16 September 2024. This work was supported in part by the National Key Research and Development Plan "NQI Integrated Services Common Technologies Research" special project under Grant 2021YFF0600100 and in part by the National Natural Science Foundation of China under Grant 41871368. *(Corresponding author: Wangshan Yang.)*

Wangshan Yang is with the College of Information Engineering, China Jiliang University, Hangzhou 310018, China (e-mail: yangwsh@whu.edu.cn).

Yongjun Zhang and Xinyi Liu are with the School of Remote Sensing and Information Engineering, Wuhan University, Wuhan 430079, China (e-mail: zhangyj@whu.edu.cn; liuxy0319@whu.edu.cn).

Boyong Gao is with the College of Information Engineering, China Jiliang University, Hangzhou 310018, China (e-mail: gaoby@cjlu.edu.cn).

Digital Object Identifier 10.1109/TGRS.2024.3430076

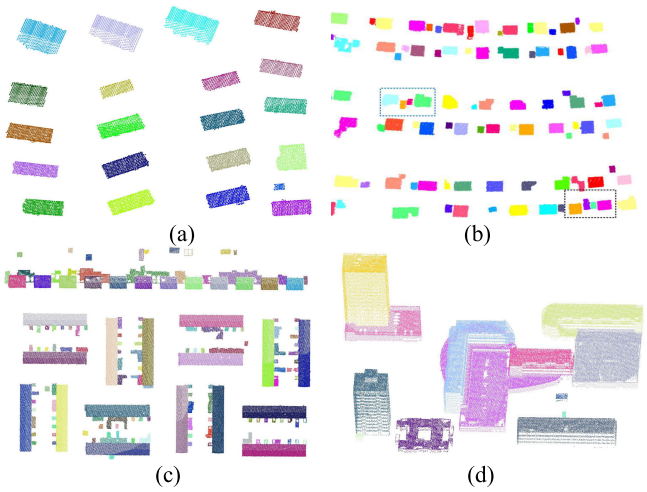

Fig. 1. Building scenes. (a) Distance between buildings is much larger than the point cloud point spacing. (b) Some building spacing is close to the point cloud point spacing. (c) and (d) Multiple buildings are connected in some way.

3-D building models must possess physical distinguishability. An individual building is defined as the prominent ground portion that lacks any common set (common connection) with other buildings and cannot be distinguished through computer vision techniques [3], [4].

Currently, there exist numerous traditional and state-of-the-art deep learning methods for point cloud classification, building point cloud extraction, and other related tasks. However, the research on building individual segmentation remains relatively limited and predominantly relies on traditional approaches. Despite the satisfactory outcomes achieved by existing building individual segmentation methods, they still exhibit certain limitations. The majority of these methods, including Euclidean distance clustering segmentation [5], voxel-based segmentation algorithms [6], move window algorithms [7], and density-based spatial clustering algorithms [8], demonstrate satisfactory performance when the distance between buildings is significantly larger than the point cloud point spacing. However, in the case of buildings situated in complex scenes, existing building individual segmentation methods often encounter challenges related to high rates of undersegmentation and oversegmentation. In such complex scenes, most buildings are interconnected, with certain building distances surpassing the point spacing, while others are closer to it. The roof of each building is typically composed of one or more planes, with complex topological and convex–concave relationships. When roof planes are extracted and their topological and convex–concave relationships are analyzed, it becomes challenging to ascertain which planes belong to the same building solely based on these relationships. To enhance the accuracy of building individual segmentation in complex scenes, this article proposes a scene adaptive approach for building individual segmentation using large-scale airborne LiDAR point clouds. The main contributions of this study are given as follows.

1) We quantify the complexity of building groups by establishing a cylindrical neighborhood graph among objects.
2) Utilizing the graph-cut algorithm, we classify the buildings based on the cylindrical neighborhood graph derived from the objects.
3) We propose a scene adaptive building individual segmentation (SABIS) based on large-scale airborne LiDAR point clouds. The algorithm classifies buildings into urban scene buildings and rural residential area buildings based on their characteristics. Appropriate methods of building individual segmentation are employed for different types of buildings.

We propose an SABIS based on large-scale airborne LiDAR point clouds. The method first uses the moving window (MW) algorithm to segment building point clouds into groups of building point clouds. Following this, these group point clouds are further segmented into roof point clouds and facade point clouds. The roof point clouds are then segmented into roof objects using an object segmentation method. Next, we extract the area feature and elevation feature of each roof object. Using these features—specifically, the elevation feature and projected area feature of the roof object—we classify the building point clouds into two categories: urban scene buildings and rural residential scene buildings. For urban scene buildings, we apply a building individual segmentation method based on the cylinder model consistency. Conversely, for rural residential scene buildings, the building individual segmentation method based on bidirectional saliency features is employed. Finally, an SABIS method based on large-scale airborne LiDAR point clouds is realized.

II. Related Work

In the field of building point clouds research, the primary focus has been on building extraction, building modeling, roof segmentation, and facade or plane segmentation. Traditional methods and deep learning methods have been widely used for these tasks. However, when it comes to building individual segmentation in point clouds, most existing methods still rely on traditional approaches. These approaches include Euclidean clustering algorithms, move window algorithms, density-based spatial clustering of applications with noise (DBSCAN) algorithms, and traditional connected component labeling (TCCL) algorithms. In recent years, many researchers have utilized the Euclidean clustering algorithm to segment building point clouds into separate clusters [5]. This method demonstrates good performance in building scenes where the distances between buildings are significantly larger than the point spacing, enabling effective building individual segmentation. However, in scenes with multiple connected buildings, it may encounter challenges such as undersegmentation or oversegmentation of building individuals. To address this, the move window algorithm is employed to segment the filtered LiDAR point cloud into clusters, with each cluster representing an individual building or tree [7]. Following this, a step is taken to remove trees from the point cloud clusters, refining the segmentation process. Cao et al. utilized the DBSCAN algorithm to achieve individual building segmentation [8], [9]. Du et al. [2] proposed an enhanced version of the

DBSCAN algorithm specifically designed for building individual segmentation, which performs well in scenarios where the distances between buildings are significant or for small buildings. Yan and Wei [10] proposed a building individual segmentation method based on dense matching point clouds. This method extracts roof point clouds and projects them onto a 2-D grid. By utilizing the topological relationships between grid cells, individual building point clouds are obtained. The traditionally connected component labeling algorithm can effectively achieve roof individual segmentation by the open-source software CloudCompare [2]. Matei et al. [6] utilized a 3-D voxel algorithm to segregate point clouds into ground and nonground points, followed by a smaller 3-D voxel algorithm applied to segment nonground points and eliminate vegetation from point cloud clusters, thus realizing building individual segmentation. Gao and Yang [11] proposed a building individual segmentation method for mobile laser scanning (MLS) point clouds that utilize gaps in the point cloud histogram to segment individual buildings. However, the assumption of buildings being parallel to the MLS trajectory may not always be valid. Xia and Wang [12] proposed a method for building individual segmentation of MLS point clouds, which uses a building facade for building location. Then, the original point cloud is divided into clusters, each containing a potential building. Finally, bearing similarity to the method outlined in [11], a point-counting contour following the rectangle is constructed. The building cluster contours are segmented at the lowest bin, hence accomplishing building individual segmentation. Wang et al. [13] proposed a building individual segmentation method that combines the random sample consensus (RANSAC) algorithm and the DBSCAN algorithm. Zeng et al. [14] presented a method for extracting individual building facades from data collected by mobile mapping systems, significantly improving efficiency of the algorithm. Ural and Shan [15] proposed a method where the roof point clouds are obtained by calculating the normal of points within the neighborhood of each point and using the angle between each point's normal vector and the horizontal direction as a threshold. Following this, the DBSCAN clustering algorithm is then applied to label the individual building.

III. Methodology

In this article, we propose an SABIS based on large-scale airborne LiDAR point clouds. First, the method uses the MW algorithm to segment building point clouds into building group point clouds, which are subsequently segmented into roof point clouds and facade point clouds. Second, the roof point clouds are segmented into roof objects. Then, area feature and elevation feature of the roof object are extracted, and the building groups are classified into urban scene buildings and rural residential scene buildings based on these features of the roof object. Finally, for urban scene buildings, the building individual segmentation method based on the cylinder model consistency is used. For rural residential scene buildings, the building individual segmentation method based on bidirectional saliency features is employed. The workflow of the SABIS algorithm is shown in Fig. 2.

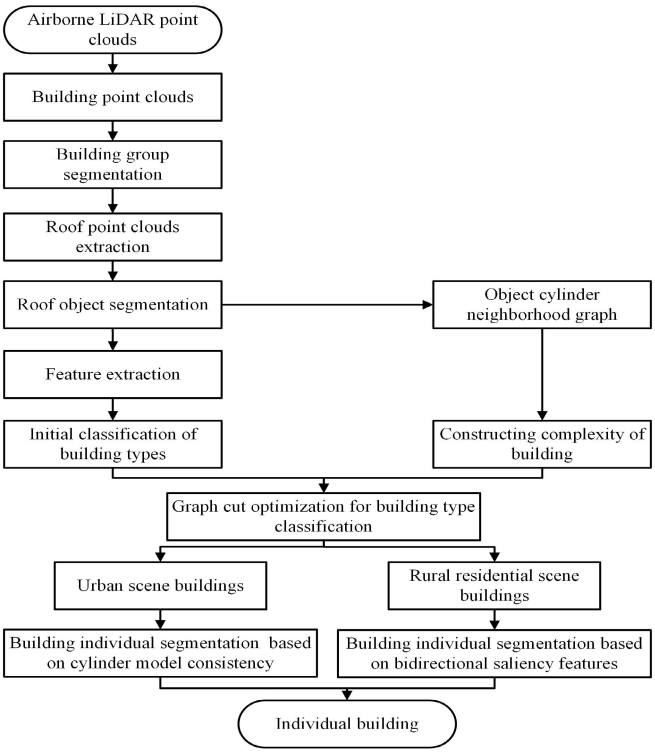

Fig. 2. Workflow of the SABIS algorithm.

A. Building Group Segmentation

During the design of buildings, it is crucial to consider factors such as lighting and ventilation, as well as maintaining an appropriate distance between buildings. In this section, based on the characteristics of the spacing between buildings, we introduce the MW algorithm [7] to segment the building point cloud into clusters and identify and merge isolated point cloud clusters, thereby achieving building grouping segmentation.

1) Building Point Cloud Cluster Segmentation: Sampath and Shan (2007) proposed an MW clustering algorithm used for individual building segmentation. In subsequent studies, Awrangjeb and Fraser [16] and Mohammad and Clive [7] also applied the algorithm to achieve individual building segmentation. This algorithm segments the building point cloud into individual buildings based on the connectivity characteristics of point cloud in 2-D space. In this article, considering the efficiency and segmentation accuracy of the algorithm, we apply the MW algorithm to segment the building point cloud into clusters and then merge isolated point cloud clusters to achieve the segmentation of building groups. For the Ningbo and AHN3 datasets, the thresholds are set to 1.5 and 0.2, respectively.

2) Recognition of Isolated Point Cloud Clusters: After using the MW clustering algorithm for building point cloud segmentation, sparse local point clouds might emerge due to factors, such as reflections from building materials. The MW clustering algorithm may segment some sparse point clouds into isolated point cloud clusters. To address this issue, this study determines whether a point cloud cluster is isolated based on the calculation of its area. For isolated point cloud

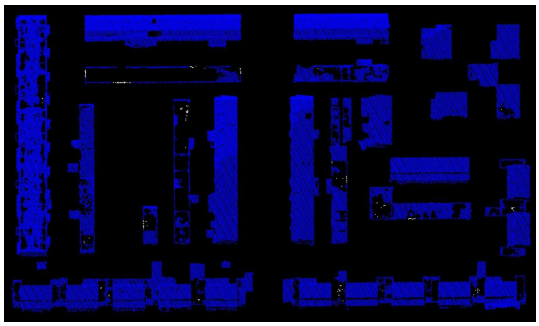

Fig. 3. Isolated point cloud cluster.

clusters, the nearest building cluster is identified, and the isolated point cloud cluster is merged into the closest building cluster, accomplishing in the merging of isolated point cloud clusters.

Guo et al. [17] investigated the technique of projecting point clouds from neighborhood areas onto variously oriented planes, thereby capturing side views or profiles of the clouds. Building upon this technique, our study calculates the horizontal projected area of point cloud clusters. This involves projecting the clusters onto a horizontal grid (*xoy* plane) and estimating the cluster area based on the cells occupied by the grid. The pseudocode for this calculation is given as follows.

Notation:
Pc: point cloud cluster;
dc: grid size;
$area$: point cloud cluster area;
Input: pc, dc, $area$;
Output: $area$;
For $i = 1, 2, \ldots, m$, do
Starting from the ith point cloud cluster, the maximum (max_x, max_y, max_z) and minimum (min_x, min_y, min_z) of this point cloud cluster are calculated.
According to the point spacing dc and the maximum and minimum values of the point cloud cluster, the number of rows $nx(nx = (int)((max_x - min_x)/dc) + 1)$ and the number of columns $ny(ny = (int)((max_y - min_y)/dc) + 1)$ of the grid are calculated.
The point cloud is filled into the grid, marking the grid with the point as true. The number of the grid is counted and the area of the point cloud cluster is calculated according to the number of grid and grid size.
Output: point cloud cluster area.

For each point cloud cluster, compute its area and determine whether it is isolated based on the computed area. Fig. 3 illustrates local isolated clusters around buildings, with blue points indicating segmented building clusters and white points marking the isolated clusters. These isolated clusters are then merged with the nearest building clusters.

3) Merging of Isolated Point Cloud Clusters: Isolated clusters are typically homogeneous. Occasionally, some may be surrounded by others, making it crucial to calculate their distance to the nearest building group and merge them accordingly. This prevents oversegmentation of building groups. This study employs a Kd-tree structure from the Point Cloud Library (PCL) to compute the shortest distance between each point in the isolated clusters and their nearest building groups. The pseudocode for this process is given as follows.

Notation:
Input:
IPcc: Isolated point cloud cluster;
BPcc: building point cloud cluster;
Output:
MPcc: Merged building point cloud cluster;
Construct a Kd-tree for all building point cloud cluster using PCL.
For each point in an isolated point cloud cluster, identify the nearest neighbor within a building group, noting the group label and the distance dis.
For $i = 1, 2, \ldots, m$, do
Find the minimum distance dis between all points of isolated cluster and building groups.
Calculate the minimum value dis_{min} of dis, and the corresponding group label.
Point cloud cluster is merged into the corresponding building group of dis_{min}.
Continue until all isolated clusters have been merged with the nearest building group.
Output: Merged building point cloud cluster.

B. Roof Point Cloud Extraction

Roof structures of buildings can be complex, with both regular and irregular features. Plane segmentation algorithms attempting to identify roof points can sometimes misclassify them. In this article, we compute covariance matrices, eigenvalues, and eigenvectors for k-nearest neighbor point sets, using these to assess linear, planar, and spherical characteristics through eigenvector analysis. The roof point clouds that are extracted from merged building point cloud cluster roof point clouds are extracted from merged building point cloud cluster. The steps are given as follows.

Assume that $A = \{P_j i = 1, 2, \ldots, N\}$ represents building point cloud, where $P_j = (x_i, y_i, z_i)$ represents the 3-D coordinates of the point cloud and N represents the number of points in the point cloud. A Kd-tree is created for this point cloud, and the k-nearest neighbors of point P_j are found. The centroid is calculated for the k points according to the following equation:

$$\bar{X} = \frac{\sum_{i=1}^{N} x_i}{N}, \quad \bar{Y} = \frac{\sum_{i=1}^{N} y_i}{N}, \quad \bar{Z} = \frac{\sum_{i=1}^{N} z_i}{N} \tag{1}$$

where $P(\bar{X}, \bar{Y}, \bar{Z})$ represents the centroid of the point cloud. The covariance matrix C of the k neighboring points is calculated based on the centroid, as shown in the following equation:

$$C = \begin{pmatrix} \mathrm{cov}(x,x) & \mathrm{cov}(x,y) & \mathrm{cov}(x,z) \\ \mathrm{cov}(y,x) & \mathrm{cov}(y,y) & \mathrm{cov}(z,y) \\ \mathrm{cov}(z,x) & \mathrm{cov}(z,y) & \mathrm{cov}(z,z) \end{pmatrix} \tag{2}$$

where $\mathrm{cov}(x,y)$, $\mathrm{cov}(x,z)$, $\mathrm{cov}(y,x)$, $\mathrm{cov}(y,z)$, $\mathrm{cov}(z,x)$, and $\mathrm{cov}(z,y)$ represent covariance; and $\mathrm{cov}(x,x)$, $\mathrm{cov}(y,y)$,

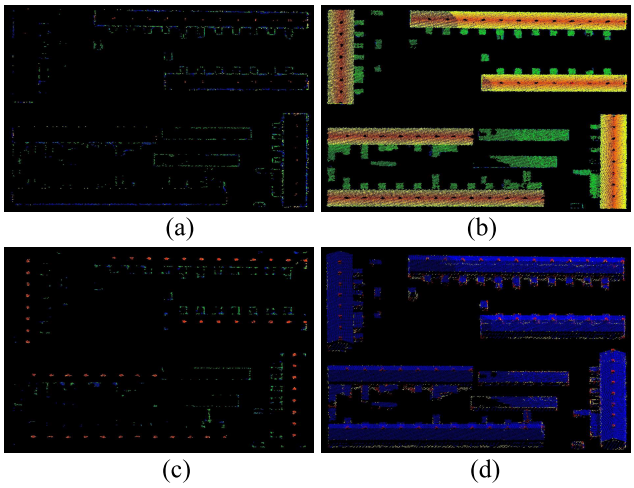

Fig. 4. Local linear, planar, and spherical point clouds of buildings. (a) Linear point clouds, (b) planar point clouds, (c) spherical point clouds, and (d) overall effect of linear, planar, and spherical point clouds.

and $\mathrm{cov}(z, z)$ represent variance. Assuming that λ_j is the jth eigenvalue of the covariance matrix $[j \in (1, 2, 3)]$ and $\vec{v}_j$ is the jth eigenvector, the calculation of the eigenvalue is shown in the following equation:

$$C \cdot \vec{v}_j = \lambda_j \cdot \vec{v}_j, \quad (\lambda_1 \geq \lambda_2 \geq \lambda_3). \tag{3}$$

Among them, the three eigenvalues $(\lambda_1 \geq \lambda_2 \geq \lambda_3)$ of the covariance matrix represent the fitting residuals along three directions. By utilizing the three eigenvalues of the covariance matrix, linear, planar, and spherical point clouds are computed. The local linear, planar, and spherical point clouds of buildings are illustrated in Fig. 4, with different colors assigned based on their elevation. Fig. 4(d) displays the collective effect of linear, planar, and spherical point clouds, with the colors yellow, blue, and red representing them, respectively. Based on the three eigenvalues of the covariance matrix, the calculation formulas for linear, planar, and spherical point clouds are shown in the following equations:

$$\alpha_{1d} = \frac{\sqrt{\lambda}_1 - \sqrt{\lambda}_2}{\sqrt{\lambda}_1}, \quad \alpha_{2d} = \frac{\sqrt{\lambda}_2 - \sqrt{\lambda}_3}{\sqrt{\lambda}_1}, \quad \alpha_{3d} = \frac{\sqrt{\lambda}_3}{\sqrt{\lambda}_1} \tag{4}$$

$$V_l = \underset{x \in [1,3]}{\arg \max}(\alpha_{xd}). \tag{5}$$

Among them, $\lambda_1, \lambda_2, \lambda_3 (\lambda_1 \geq \lambda_2 \geq \lambda_3)$ are the eigenvalues of the covariance matrix for each point's k-nearest neighbor point set. Based on the linear feature ($V_l = 1$ indicating that the k-nearest neighbor point set of the point is linear), planar feature ($V_l = 2$ indicating that the k-nearest neighbor point set of the point is planar), and spherical feature ($V_l = 3$ indicating that the k-nearest neighbor point set of the point is spherical), building point clouds is segmentation. If the k-nearest neighbor point set of a point forms a plane, the angle θ_1 between the plane normal vector and the vertical direction is calculated. This angle θ_1 is used to determine whether the point belongs to the facade point cloud, as shown in the following equations:

$$\theta_1 - 90^\circ \leq \theta_2, \quad (90^\circ \leq \theta_1 \leq 180^\circ) \tag{6}$$

$$90^\circ - \theta_1 \leq \theta_2, \quad (0^\circ \leq \theta_1 \leq 90^\circ) \tag{7}$$

where θ_2 is the angle threshold between normal vector of facade point clouds and horizontal plane, and the threshold for θ is set to 30°. If (6) or (7) holds, the point is categorized as a facade point cloud. Otherwise, it is categorized as a roof point cloud. If the k-nearest neighbor point set of a point is linear or spherical, it is classified as a roof point. The local schematic of the roof point cloud is shown in Fig. 5.

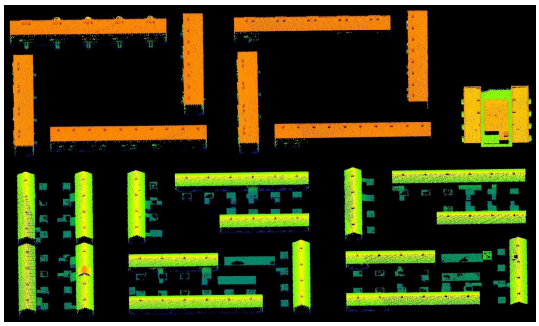

Fig. 5. Local roof point clouds.

C. Roof Object Segmentation

Commonly used object segmentation methods include the mean shift clustering algorithm and the density-based clustering algorithm (DBSCAN). The mean shift clustering algorithm does not require specifying the number of clusters and can handle clusters of arbitrary shapes, but it is sensitive to the bandwidth parameter [18]. On the other hand, the DBSCAN algorithm is versatile in handling clusters of arbitrary shapes and sizes, but it requires relatively uniform point cloud density [19]. Due to the uniform density of the airborne LiDAR building roof point clouds and the sparse density of the building facade point clouds, there exists a significant variation in point cloud density across different parts of the building. In this article, we apply a density-based object segmentation method [4]. This method does not consider core points, border points, and noise points, instead clustering points based on density features. This approach prevents distant points from being erroneously segmented into the same object and facilitates disconnection between points belonging to different objects. The roof point cloud is segmented into individual roof objects using the aforementioned object segmentation method. The local schematic illustrating the roof objects is shown in Fig. 6, with each color representing a distinct object. For the Ningbo and AHN3 datasets, the thresholds are set to 1.2 and 0.8, respectively.

D. Feature Extraction

In 3-D space, point clouds are scattered, and features and local neighborhood features of each point are limited. To effectively classify building groups, it is essential to compute the features of each roof object. This study selects two key features

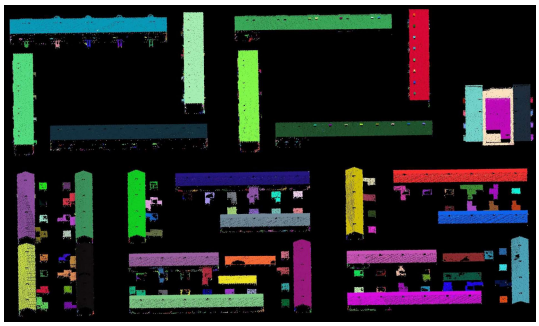

Fig. 6. Locally classified roof objects.

of roof objects: the area feature and the elevation feature. The elevation feature of the roof object is calculated by using the building point cloud cluster, and the elevation value of building point cloud cluster is assigned to the elevation of roof object (referred to as height_C). Given that airborne LiDAR point cloud data are typically normalized before classification, with the lowest point of the building being normalized to the same plane, the classification of whether a building belongs to an urban or a rural area is based on the maximum elevation of each object. Generally, a higher roof object of a building indicates a higher possibility of it being an urban scene building. For building point cloud clusters, a roof point cloud extraction method and a roof point cloud object segmentation method are used to obtain roof objects. The roof object area feature is a crucial feature. For the calculation of the roof object area feature (denoted as area_C for the current roof object), the projected area method is employed.

E. Building Group-Type Classification

1) Initial Classification of Building Group Types: Existing methods for building group-type classification are based on the functionality and application requirements of buildings. Traditional and deep learning methods are utilized to classify buildings using point cloud data and remote sensing images, focusing on the features of their roofs. However, buildings segmented as a building group often consist of multiple roofs, and the relationships between these roofs significantly impact building group-type classification. To adapt to the segmentation of individual buildings, this article proposes a building group-type classification method based on an object cylinder neighborhood graph. Subsequently, the building groups are categorized into urban scene buildings and rural residential scene buildings. The specific steps of this method are given as follows. First, the building point cloud is divided into building groups according to the building group segmentation. Second, the roof point cloud cluster extraction method and object segmentation method are used to obtain the roof objects. Finally, the elevation features and area features are calculated, and the buildings are initially classified based on these features.

2) Building Type Classification by Graph Cut Optimization Algorithm: Graph cut is a classical image segmentation method, which is widely used in computer vision, image segmentation, medical image analysis, and so on [20]. The principle is to map an image into a graph and then achieve image segmentation according to the maximum flow and minimum cut algorithm. Graph cut has received much attention as an energy minimization method, and its first appearance in the field of computer vision was described in 1999 [21]. It was later explained and extended in detail [22], [23]. Graph cut aims to transform low-level computer vision problems, such as image restoration [24], image segmentation [25], and point cloud segmentation [26], which were transformed into labeling problems. In point cloud segmentation, each point $p \in P$ is assigned a label l from L. The meaning of the label l varies with different problems, and it can be image restoration [24], image segmentation [25], building roof segmentation [26], [27], and building extraction [28], [29].

A building is generally composed of one or multiple roof objects, and multiple objects that form a building are typically connected by building facades. The greater the elevation of each roof object, the higher the likelihood that the building has a greater elevation complexity, indicating that it is an urban scene building. The smaller the ratio of the sum of neighboring objects' areas to the product of their areas and the roof object, the more likely it is that adjacent objects belong to separate individual buildings. Consequently, the area complexity of the building is higher. In the following, we optimize the initial classification results of building types by constructing the elevation complexity and area complexity of the buildings and applying a graph cut optimization algorithm.

For each point $p \in P$ in the building point cloud, a label $l \epsilon L$ is assigned to solve the labeling problem, which can be defined by an energy function. The label assignment for point p is obtained by minimizing the energy function, which typically includes two parts, as shown in the following formula:

$$E(f) = E_{\text{data}}(f_p) + \delta E_{\text{smooth}}(f_{pq}) \tag{8}$$

where $p, q \in N$, and $p \neq q$, in which p represents the center object and q represents an object within the cylindrical neighborhood radius of the central object p. N denotes the object set, and $p \neq q$ indicates that objects p and object q are different objects. In this expression, δ is a constant factor used to adjust the weight between the data cost and the smooth cost. The δ threshold is set to 3 by experimenting with the dataset. The data cost [the first term in (8)] determines the likelihood of a building group being an urban scene building based on maximum elevation of object elevation. A larger object elevation results in a smaller data cost value, indicating a greater possibility that the building group is an urban scene building. The smooth cost [the second term in (8)] measures the consistency of object areas. A smaller difference in area between the central object and its neighboring objects leads to a smaller smooth cost value, indicating a higher possibility that the building group is an urban scene building.

The data cost penalizes the elevation of each roof object in the building group. The data cost is constructed based on the relationship between the elevation of objects within the building group and a height threshold, reflecting the elevation complexity of the building group. The formulation of the data cost term is shown in the following equation:

$$E_{\text{data}}(f) = \exp^{\frac{\text{height}_T}{\text{height}_C}} \tag{9}$$

where height_T represents the height threshold of urban scene building group and height_C represents the height value of the building roof object.

The smoothness cost penalizes the consistency of areas between neighboring objects within the same building group. According to the object cylinder neighborhood graph, the relationship between the roof objects is established to find the neighboring objects of the center roof. The method for constructing the object cylinder neighborhood graph between roof objects is used [4]. The smoothness term is constructed based on the ratio of the sum of the roof object areas within the neighborhood radius of the central roof object to the product of the roof object areas within the same neighborhood radius. This ratio represents the relationship between the areas of the roof objects within the building group. The formulation of the smoothness term is shown in the following equation:

$$E_{\text{smooth}}(f) = \exp^{\frac{(\text{area}_C+\text{area}_N)*\text{area}_T}{\text{area}_C*\text{area}_N}} \tag{10}$$

where area_T represents the area threshold of urban scene building group roof object, area_C represents the area of current building roof object, and area_N represents the area of cylinder neighborhood object of current building roof object.

The energy function is constructed according to formula (8), and the graph cut algorithm is used to optimize the initial classification results of building types, classifying the buildings into urban scene buildings and rural residential scene buildings.

F. Building Individual Segmentation

According to the method of building type classification, the airborne LiDAR building point cloud is classified into urban scene buildings and rural residential area buildings. Then, for urban scene buildings, the building individual segmentation method based on the cylinder model consistency is applied. For rural residential area buildings, the building individual segmentation method based on bidirectional visual saliency features is utilized. Ultimately, SABIS based on large-scale airborne LiDAR point clouds is achieved.

1) Building Individual Segmentation Method Based on the Cylinder Model Consistency: Urban buildings are important places for human life, entertainment, and work, and it is of great significance to perform individual segmentation on these large-scale buildings. Urban buildings are generally composed of one or more individual buildings, each with complex structures and a relatively large footprint. It is necessary to merge the segmented small point cloud clusters. In response to urban scene building, this article uses building individual segmentation method based on cylinder model consistency [3]. The flowchart of the building individual segmentation method based on cylinder model consistency is shown in Fig. 7. First, Fig. 7(a) and (b) represents the aerial images corresponding to inputted building point clouds and inputted building point clouds, respectively. Second, based on the Ikd-2DSNN algorithm, the building point clouds are divided into individual building (individual building means that a point clouds cluster only contains one building) and podium building (podium building means that a point clouds cluster contains multiple buildings), as shown in Fig. 7(c) and (d). Third, the octree-based regional growing is used to remove façade point clouds from the podium building, as shown in Fig. 7(e). Fourth, based on the Ikd-3DSNN algorithm, podium building roof planes from the podium building are divided into individual building roof, as shown in Fig. 7(f). Fifth, according to the characteristics of building facade directly below the building roof, building façade point cloud is merged into individual building roof, as shown in Fig. 7(g). Sixth, according to the characteristics of roof detail above the roof and individual building roof MBR size, the roof detail cluster is recognized and merged into individual building, as shown in Fig. 7(h). Finally, isolated point cloud cluster is merged into the nearest neighbor individual building, as shown in Fig. 7(i).

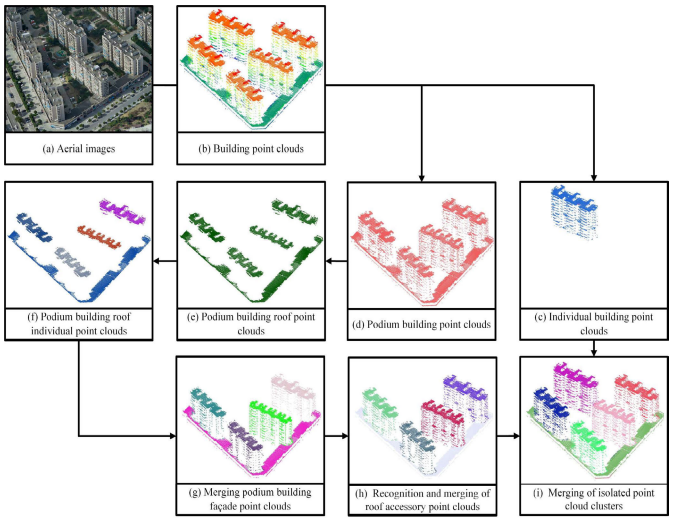

Fig. 7. Illustration of the UBIS method. (a) Aerial images corresponding to inputted building point clouds, (b) inputted building point clouds, (c) toutput of single-building instance, (d) output of multibuilding instances, (e) output of multibuilding roof planes, (f) output of single-building roof instance, (g) output of merging of building façade point clouds, (h) recognition and merging of roof detail cluster, and (i) output of isolated point cloud cluster merged into building instance.

2) Building Individual Segmentation Method Based on Bidirectional Saliency Features: In rural residential areas, the buildings generally have low floors, small footprints, simple structures for each individual building, independent characteristics, and relatively small height differences between buildings, and most buildings are connected in some way. The distance between some buildings may be greater than the point spacing, while others are close to the point spacing. The roofs of each rural residential area building are typically composed of one or more planes, with complex topological and concave–convex relationships. It is difficult to determine which planes belong to the same individual building based solely on the topological and concave–convex relationships between the planes if the roof planes are extracted, and then, their topological and concave–convex relationships are evaluated. In response to these rural residential area buildings, this article uses a building individual segmentation based on bidirectional saliency features [4]. In this method, the building point cloud is divided into building facade point cloud and

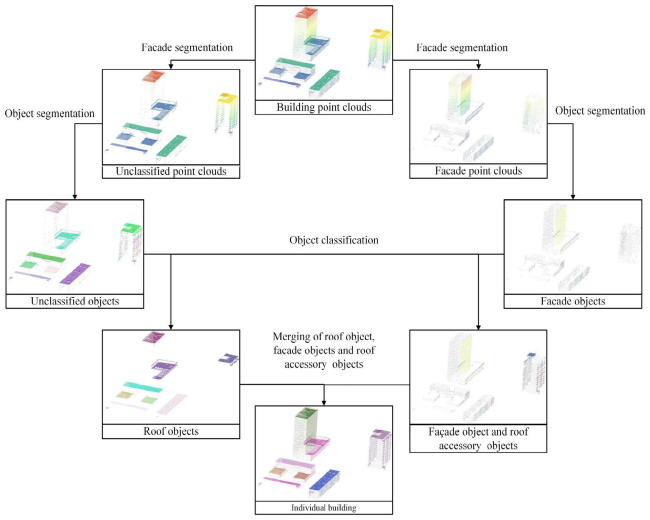

Fig. 8. Illustration of the building individual segmentation method based on bidirectional saliency features.

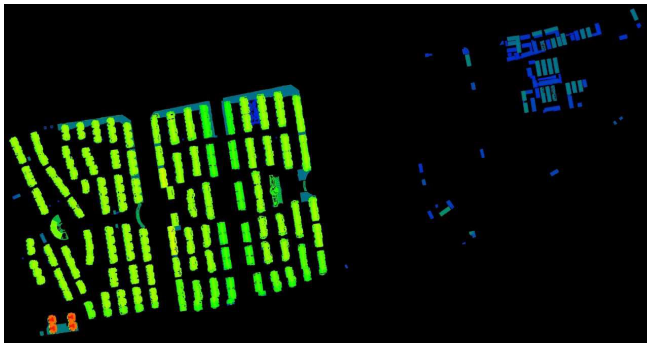

Fig. 9. Dataset1 building point clouds.

unclassified point cloud. For building facade point cloud and unclassified point cloud, the object segmentation method and the object classification method are used to divide the small building group into the homogeneous roof object, facade object, and roof auxiliary structure object. The cylinder model consistency, cylinder model consistency difference features of the roof object facade objects and roof accessory objects, and 2-D Euclidean distance features between adjacent objects of roof objects, facade objects, and roof accessory objects are extracted; then, the objects are merged and updated according to the features to realize the building individual segmentation. Fig. 8 illustrates the pipeline of the building individual segmentation method based on bidirectional saliency features.

IV. Experimental Results and Analysis

A. Data Introduction

Dataset1 and dataset2 refer to the Ningbo datasets, as depicted in Figs. 9 and 10, respectively. The value of the verticality is represented with a color map going from blue to green to red. In the Ningbo dataset, the average LiDAR point cloud has a point spacing of approximately 0.35 m, while the median point density of building point clouds is 8 points/m^2, which includes classification information. Dataset1 comprises

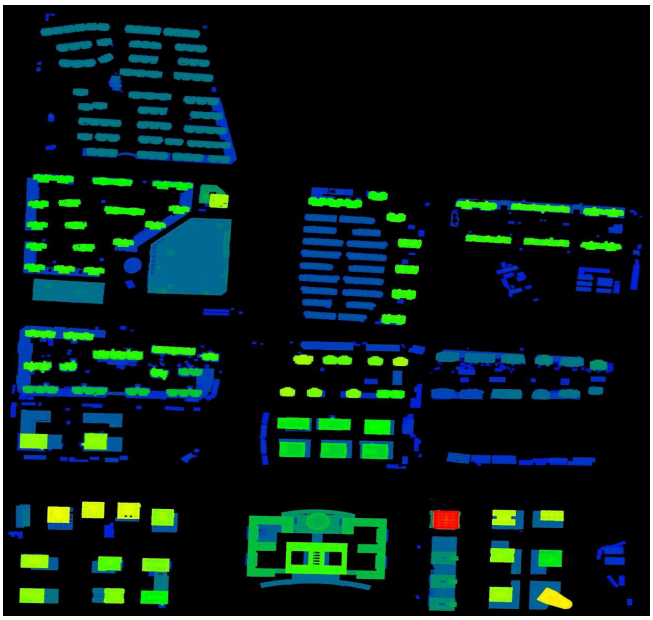

Fig. 10. Dataset2 building point clouds.

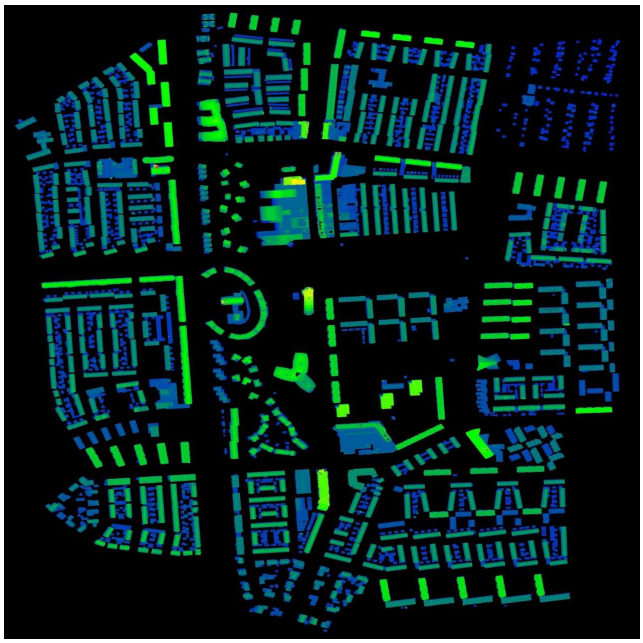

Fig. 11. Dataset3 building point clouds.

6 588 490 points, which include 831 678 points corresponding to buildings and a total of 182 buildings. The entire dataset covers an area of approximately 0.53 km^2. Dataset2 consists of 3 098 649 points, encompassing 309 864 points corresponding to buildings, with a total of 392 buildings. The entire dataset covers an area of approximately 1.3 km^2. The entire Ningbo dataset comprises an airborne LiDAR point cloud predominantly capturing urban scene buildings, including both low- and high-rise structures, with a relatively large area dedicated to high-rise buildings.

Dataset3 refers to the Dutch AHN3 dataset, as represented in Fig. 11. The LiDAR dataset used in this article was a published benchmark dataset, which was classified as

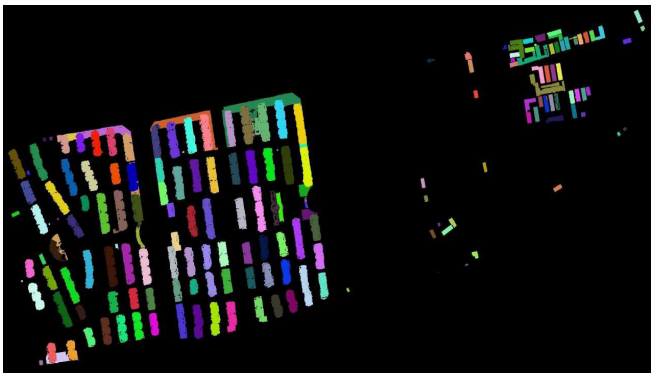

Fig. 12. Result of the dataset1 building individual segmentation.

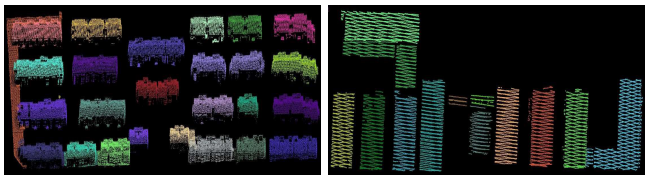

(a) (b)

Fig. 13. Result of the dataset1 local building individual segmentation result. (a) Results of urban scene buildings individual segmentation in the blue rectangle. (b) Results of rural residential scene buildings individual segmentation in the red rectangle.

buildings. The AHN3 dataset is freely available to the public.[1] The dataset primarily comprises an airborne LiDAR point cloud capturing rural residential scene buildings. It includes both low- and high-rise buildings, with a significant presence of complex interconnected rural residential scene buildings. The dataset includes a total of 34 395 134 points, with 5 935 964 points corresponding to buildings and consists of 2239 buildings. Classification information is provided within the dataset. The entire building scene covers an area of approximately 2.2 km^2.

The airborne LiDAR point cloud dataset used in this experiment includes reflection intensity, echo times, and classification information. The classification information primarily includes ground, trees, buildings, bridges, and other objects. This experiment will utilize the building point clouds from both the Ningbo dataset and the Netherlands AHN3 dataset to validate the performance of the SABIS algorithm as proposed in this article.

B. Result of Building Individual Segmentation

The SABIS algorithm in this article is used for building individual segmentation in dataset1, and the individual segmentation results are shown in Fig. 12, in which the blue rectangle and red rectangle are shown in Fig. 13(a) and (b), respectively. Fig. 13(a) shows the individual segmentation result of an urban scene building. The building scene includes a podium building connected by multiple buildings and buildings whose distance between buildings is much larger than the distance between points in point clouds. Fig. 13(b) shows the individual segmentation result of a rural residential scene

[1]https://www.pdok.nl/nl/ahn3-downloads

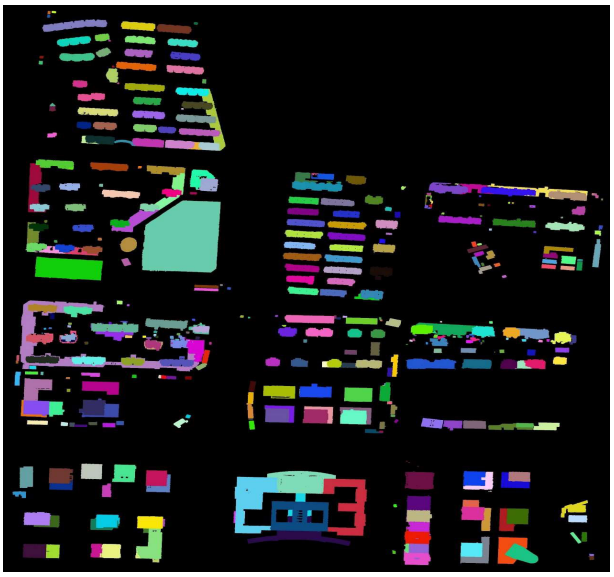

Fig. 14. Result of the dataset2 building individual segmentation.

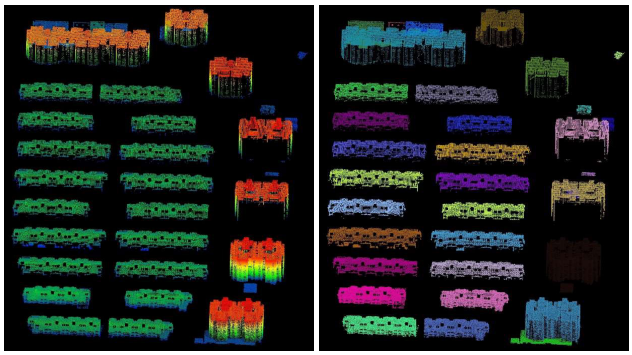

(a) (b)

Fig. 15. Result of the dataset2 urban scene building individual segmentation in the blue rectangle. (a) Building point clouds and (b) result of building individual segmentation.

building. The building scene contains multiple connected buildings. The SABIS algorithm proposed in this article demonstrates good applicability for both urban scene buildings as shown in Fig. 13 and rural residential scene buildings as shown in Fig. 13(b). The total building scene coverage area of dataset1 is about 0.53 km^2, and the building types in the scene range are complex. However, dataset1 is segmented by the SABIS algorithm in this article, and satisfactory results are obtained.

Building individual segmentation of dataset2 was performed using the SABIS algorithm proposed in this article, and the results are depicted in Fig. 14. The segmentation outcomes highlighted in the blue rectangle, red rectangle, and yellow rectangle are displayed in Figs. 15–17, respectively. Figs. 15 and 16 illustrate the segmentation results of buildings in an urban scene. The building scene includes the podium buildings connected by multiple buildings, buildings whose distance between buildings is much larger than the distance between points in point clouds. Fig. 17 shows the segmentation result of a rural residential scene building. The building scene contains multiple connected buildings. The SABIS algorithm

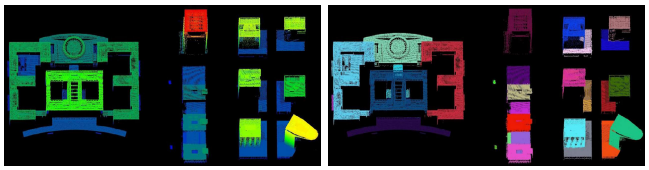

(a) (b)

Fig. 16. Result of the dataset2 urban scene building individual segmentation in the red rectangle. (a) Building point clouds and (b) result of building individual segmentation.

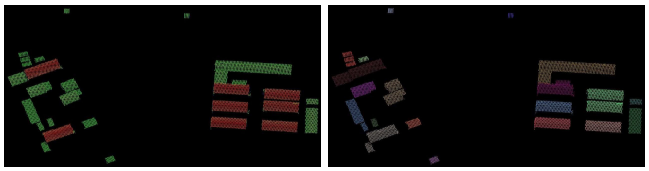

(a) (b)

Fig. 17. Result of the dataset2 rural residential scene building individual segmentation in the yellow rectangle. (a) Building point clouds and (b) result of building individual segmentation.

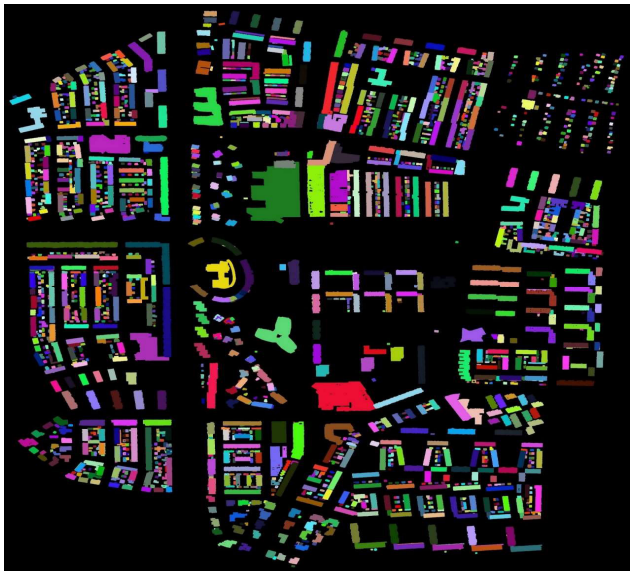

Fig. 18. Result of the dataset3 building individual segmentation.

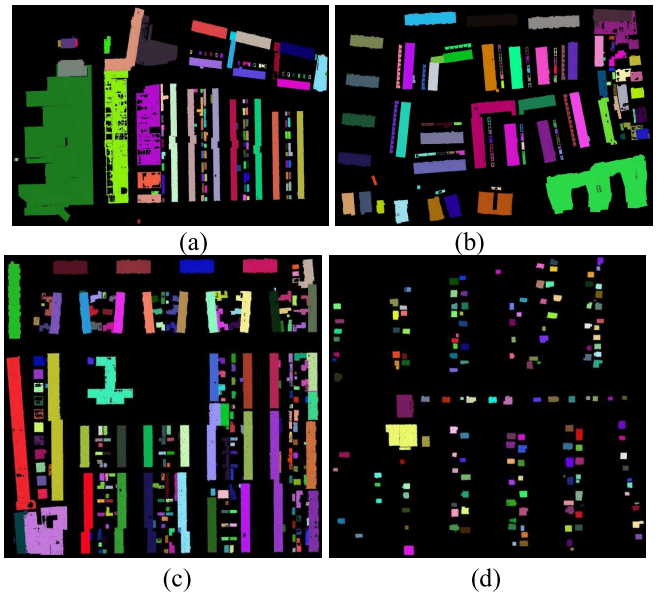

(a) (b) (c) (d)

Fig. 19. Result of the dataset3 local building individual segmentation. (a) Result of building individual segmentation in the purple rectangle, (b) result of building individual segmentation in the red rectangle, (c) result of building individual segmentation in the green rectangle, and (d) result of building individual segmentation in the blue rectangle.

in this article has good applicability for both urban scene buildings as shown in Figs. 15 and 16 and rural residential scene buildings as shown in Fig. 17. The dataset2 is mainly urban scene buildings, and the whole building scene covers an area of about 1.3 km^2. The buildings in the scene range have different types. However, the SABIS algorithm in this study performs building individual segmentation on the dataset, resulting in a satisfactory segmentation result.

The SABIS algorithm in this article is used for building individual segmentation on dataset3, and the individual segmentation results are shown in Fig. 18, where the areas within the purple, red, green, and blue rectangles are locally scaled for display purposes, as demonstrated in Fig. 19. Fig. 19(a) corresponds to the buildings in the purple rectangle, as shown in Fig. 18. The buildings in this area are composed of urban scene building and rural residential scene buildings. The roof structure of urban scene building is extremely complex, which is composed of multiple roofs with different heights, and the roof point cloud density is extremely uneven. However, the SABIS algorithm in this article provides satisfactory building individual segmentation results. Despite the close proximity and significant variations in size among rural residential scene buildings, the segmentation results remain satisfactory. Fig. 19(b) corresponds to the buildings within the red rectangle depicted in Fig. 18. This area encompasses a mixture of both urban scene buildings and rural residential scene buildings. The height differences among the rural residential scene buildings are substantial, and the roof point cloud density of some buildings appears sparse. However, these factors have minimal impact on the accuracy of individual segmentation. Fig. 19(c) corresponds to the buildings within the green rectangle depicted in Fig. 18. All the buildings in this area are small and closely interconnected, with multiple buildings connected to each other. However, the SABIS algorithm utilized in this article delivers satisfactory results for individual building segmentation. Fig. 19(d) corresponds to the buildings within the blue rectangle, as shown in Fig. 18. The buildings within this area are all rural residential scene buildings with simple roof structures. The distance between buildings is significantly larger than the point cloud's point spacing, and the segmentation effect is very good. Dataset3 comprises a large scene, with the entire building scene covering an approximate area of 2.2 km^2. The building types in the scene range are complex. However, the SABIS algorithm in this article provides satisfactory building individual segmentation results on dataset3.

In this article, the proposed SABIS algorithm is verified by selecting three building point cloud datasets, which are about 4 km^2 and include a variety of complex urban scene buildings and rural residential scene buildings. Due to the large scene size and complex building types, the algorithm

faces significant challenges. To address this, the SABIS algorithm introduced in this article classifies buildings into two categories: urban scene buildings and rural residential scene buildings, based on their distinguishing characteristics. Specifically, for urban scene buildings, a building individual segmentation method based on cylinder model consistency is utilized. For classified as rural residential scene buildings, the building individual segmentation method based on bidirectional saliency features is used, realizing the SABIS algorithm in this article. The experimental results demonstrate that the SABIS algorithm achieves a favorable segmentation effect for diverse complex building scenes.

C. Comparative Analysis of Experiments

1) Quantitative Analysis of Building Individual Segmentation Results: In the result of building individual segmentation section, the experimental results were analyzed visually, and in the following, quantitative evaluation indicators will be used to objectively and quantitatively analyze the experimental results by the SABIS algorithm in this article. There are two primary methods for quantitative analysis: the object-based quantitative evaluation method and the point-based quantitative evaluation method. The object-based quantitative evaluation method is used to evaluate the accuracy of building individual segmentation by comparing the number of undersegmented individual buildings, the number of oversegmented individual buildings, the number of correctly segmented individual buildings with the number of automatically segmented individual buildings, and the number of ground truth individual buildings. The point-based quantitative evaluation method evaluates the accuracy of building individual segmentation according to the ratio of the number of undersegmented individual building points, the number of oversegmented individual building points, the number of correctly segmented individual building points, the number of automatically segmented individual building points and the number of ground truth individual building points. When the minimum overlap ratio of the intersection over union (IoU) between an automatically segmented individual building and the corresponding ground truth individual building is greater than or equal to 0.8, the automatically segmented individual building is considered as a correctly segmented individual building. When IoU is less than the minimum overlap threshold of 0.8, if the individual building automatically segmented corresponds to multiple ground truth labeled individual buildings, the individual building automatically segmented is undersegmented. Otherwise, the individual building is oversegmented. The completeness, correctness, undersegmentation rate, and oversegmentation rate of building individual segmentation are evaluated by the object-based quantitative evaluation method and point-based quantitative evaluation method. The object-based quantitative evaluation method and the point-based quantitative evaluation method were applied to assess various metrics of the SABIS algorithm. The metrics for the three datasets are shown in Tables I and II, where datasets1 and 2 are urban scene buildings and datasets3 is residential buildings. The various metrics presented in Tables I and II demonstrate that the SABIS algorithm proposed in this article achieves high accuracy in individual segmentation of buildings within large-scale scenes. com_{obj}, $\text{com}_{\text{point}}$, cor_{obj}, and $\text{cor}_{\text{point}}$ are all above 86%, und_{obj}, und_{obj}, $\text{und}_{\text{point}}$, and $\text{over}_{\text{point}}$ are all below 10%. The results of the object-based quantitative evaluation method and the point-based quantitative evaluation method are basically consistent. The experimental results show that the SABIS algorithm in this article has good results in building segmentation on the selected dataset.

TABLE I
SABIS METHODS' THREE DATASETS BUILDING INDIVIDUAL SEGMENTATION RESULT OF OBJECT-BASED QUANTITATIVE EVALUATION METHOD

Dataset	Buildings	cor_{obj} (%)	com_{obj} (%)	und_{obj} (%)	$over_{obj}$ (%)
Dataset1	182	86.70	89.56	6.38	6.91
Dataset2	392	86.75	91.84	4.10	9.16
Dataset3	2239	88.36	86.82	4.87	6.82

TABLE II
SABIS METHODS' THREE DATASETS BUILDING INDIVIDUAL SEGMENTATION RESULT OF THE POINT-BASED QUANTITATIVE EVALUATION METHOD

Dataset	Points	cor_{point} (%)	com_{point} (%)	und_{point} (%)	$over_{point}$ (%)
Dataset1	831678	94.66	94.66	4.28	1.06
Dataset2	3098649	90.21	90.21	7.10	2.70
Dataset3	5935964	92.92	92.92	6.54	0.55

2) Quantitative Comparative Analysis Results: The proposed SABIS method is compared with four state-of-the-art benchmark methods. The four benchmark methods include the MW method [7], the 2-D DBSCAN segmentation method (DBSCAN2D) [19], the TCCL algorithm [2], and the Euclidean clustering method (EC) [5]. The selected datasets, namely, dataset1, dataset2, and dataset3, will be utilized to conduct a quantitative analysis of the building individual segmentation results for both the four benchmark methods and the SABIS method. The minimum overlap degree used to evaluate the segmentation performance of individual building is $\text{IoU}_{0.8}$, which means that there should be a minimum overlap of 80% between the automatically segmented individual building and the corresponding ground truth individual building (Dong et al., 2018). The object-based quantitative evaluation method and the point-based quantitative evaluation method are employed to assess the performance indicators of the five building individual segmentation methods. The performance indicators for the three datasets are presented in Tables III–VIII. It can be seen from Tables III, V, and VII that $\text{und}_{\text{obj}}(\%)$ and $\text{und}_{\text{point}}(\%)$ of the TCCL method, the MW method, and the DBSCAN2D method are all relatively high, indicating that these three methods have more undersegmented individual buildings in the three scenes. It can be seen from Tables III–VIII that $\text{cor}_{\text{obj}}(\%)$, $\text{com}_{\text{obj}}(\%)$, $\text{com}_{\text{point}}(\%)$, and $\text{cor}_{\text{point}}(\%)$ of the proposed SABIS method are all the highest, and the values of $\text{und}_{\text{obj}}(\%)$, $\text{und}_{\text{point}}(\%)$, $\text{over}_{\text{obj}}\%$, and $\text{over}_{\text{point}}\%$ are close to the lowest. Then, the sum of $\text{und}_{\text{obj}}(\%)$ and $\text{over}_{\text{obj}}\%$, $\text{und}_{\text{point}}(\%)$, and $\text{over}_{\text{point}}\%$ are both the lowest. In this article, the feasibility and effectiveness of five methods are analyzed by using three sets of large scene datasets at home and abroad and four benchmark methods for quantitative

TABLE III

FIVE-METHOD BUILDING INDIVIDUAL SEGMENTATION RESULT OF THE OBJECT-BASED QUANTITATIVE EVALUATION METHOD ON URBAN SCENE BUILDINGS DATASET1

Method	cor_{obj} (%)	com_{obj} (%)	und_{obj} (%)	$over_{obj}$ (%)
EC	52.56	67.58	7.69	39.74
TCCL	66.91	51.10	11.51	21.58
MW	76.97	64.29	11.84	11.18
DBSCAN2D	85.71	62.64	13.53	**0.75**
SABIS	**86.70**	**89.56**	**6.38**	6.91

TABLE IV

FIVE-METHOD BUILDING INDIVIDUAL SEGMENTATION RESULT OF THE POINT-BASED QUANTITATIVE EVALUATION METHOD ON URBAN SCENE BUILDINGS DATASET1

Method	cor_{point} (%)	com_{point} (%)	und_{point} (%)	$over_{point}$ (%)	LR_{point} (%)
EC	64.29	59.75	29.16	6.55	7.07
TCCL	55.55	55.53	44.39	0.06	0.04
MW	60.32	60.32	39.67	0.01	**0.00**
DBSCAN2D	60.18	60.17	39.82	**0.00**	0.01
SABIS	**94.66**	**94.66**	**4.28**	1.06	**0.00**

TABLE V

FIVE-METHOD BUILDING INDIVIDUAL SEGMENTATION RESULT OF THE OBJECT-BASED QUANTITATIVE EVALUATION METHOD ON THE URBAN SCENE BUILDINGS DATASET2

Method	cor_{obj} (%)	com_{obj} (%)	und_{obj} (%)	$over_{obj}$ (%)
EC	25.38	59.18	6.67	67.94
TCCL	42.47	43.88	13.33	44.20
MW	68.31	59.95	12.79	18.90
DBSCAN2D	80.07	58.42	16.43	**3.50**
SABIS	**86.75**	**91.84**	**4.10**	9.16

TABLE VI

FIVE-METHOD BUILDING INDIVIDUAL SEGMENTATION RESULT OF THE E POINT-BASED QUANTITATIVE EVALUATION METHOD ON THE URBAN SCENE BUILDINGS DATASET2

Method	cor_{point} (%)	com_{point} (%)	und_{point} (%)	$over_{point}$ (%)	LR_{point} (%)
EC	49.70	46.65	20.45	29.85	6.14
TCCL	46.76	46.74	52.30	0.94	0.04
MW	50.18	50.18	49.77	0.04	**0.00**
DBSCAN2D	50.52	50.51	49.47	**0.01**	0.01
SABIS	**90.21**	**90.21**	**7.10**	2.70	**0.00**

TABLE VII

FIVE-METHOD BUILDING INDIVIDUAL SEGMENTATION RESULT OF THE OBJECT-BASED QUANTITATIVE EVALUATION METHOD ON THE RURAL RESIDENTIAL SCENE BUILDING DATASET3

Method	cor_{obj} (%)	com_{obj} (%)	und_{obj} (%)	$over_{obj}$ (%)
EC	79.28	69.93	9.68	11.04
TCCL	51.77	24.84	30.73	17.50
MW	69.20	66.67	7.00	23.79
DBSCAN2D	84.05	60.50	12.10	**3.91**
SABIS	**88.36**	**86.82**	**4.87**	6.82

TABLE VIII

FIVE-METHOD BUILDING INDIVIDUAL SEGMENTATION RESULT OF THE POINT-BASED QUANTITATIVE EVALUATION METHOD ON THE RURAL RESIDENTIAL SCENE BUILDING DATASET3

Method	cor_{point} (%)	com_{point} (%)	und_{point} (%)	$over_{point}$ (%)	LR_{point} (%)
EC	76.87	75.52	18.81	4.33	1.75
TCCL	52.19	52.18	47.71	0.09	0.04
MW	75.84	75.84	24.09	0.07	**0.00**
DBSCAN2D	73.13	73.11	26.82	**0.06**	0.03
SABIS	**92.92**	**92.92**	**6.54**	0.55	**0.00**

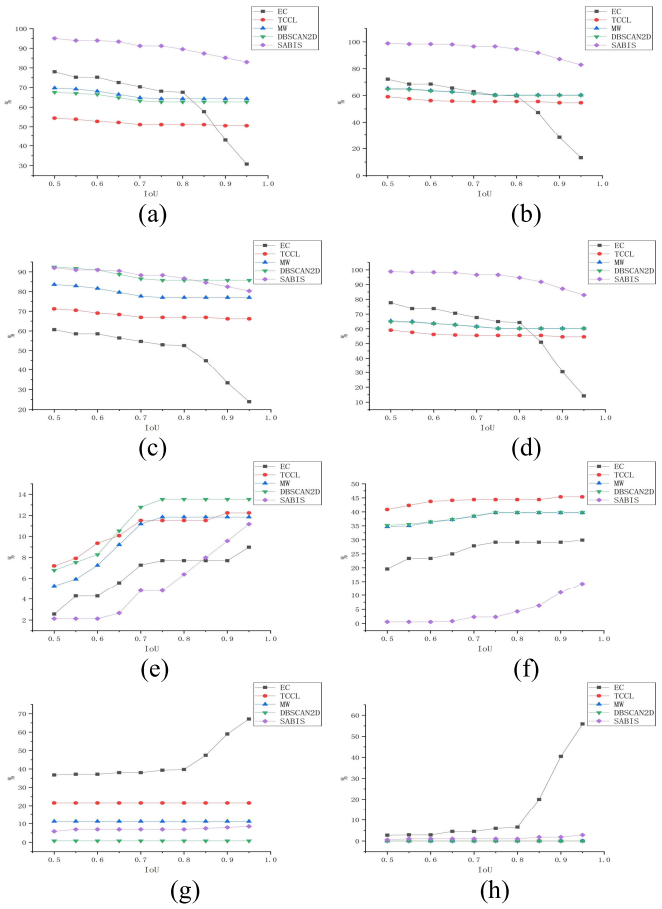

Fig. 20. Five-method segmentation dataset2 accuracy variation curves of the evaluation method based on single object and the evaluation method based on point with the increase of overlap degree. (a) Result of five-method $\boldsymbol{cor_{obj}}$ curve, (b) result of five-method $\boldsymbol{cor_{point}}$ curve, (c) result of five-method $\boldsymbol{com_{obj}}$ curve, (d) result of five-method $\boldsymbol{com_{point}}$ curve, (e) result of five-method $\boldsymbol{und_{obj}}$ curve, (f) result of five-method $\boldsymbol{und_{point}}$ curve, (g) result of five-method $\boldsymbol{over_{obj}}$ curve, and (h) result of five-method $\boldsymbol{over_{point}}$ curve.

evaluation effect. The results show that the SABIS method in this article is obviously better than the most advanced methods.

In order to analyze the performance of various building individual segmentation methods, including the selected three sets of building point cloud datasets, four currently most classic building individual segmentation methods, and the SABIS method proposed in this section, the evaluation methods based on individual object and point are applied. The changes in various accuracy indicators are examined with increasing overlap degrees to assess the performance of these building individual segmentation methods, as shown in Figs. 20–22. From Figs. 20(a), 21(a), and 22(a), it can be observed that at an overlap degree of 50%, the $\mathrm{cor_{obj}}(\%)$ value of the EC method is similar to that of the proposed SABIS method. However, as the overlap increases, the $\mathrm{cor_{obj}}(\%)$ value of the EC method rapidly decreases, indicating that both methods are significantly influenced by the overlap degree (i.e., most

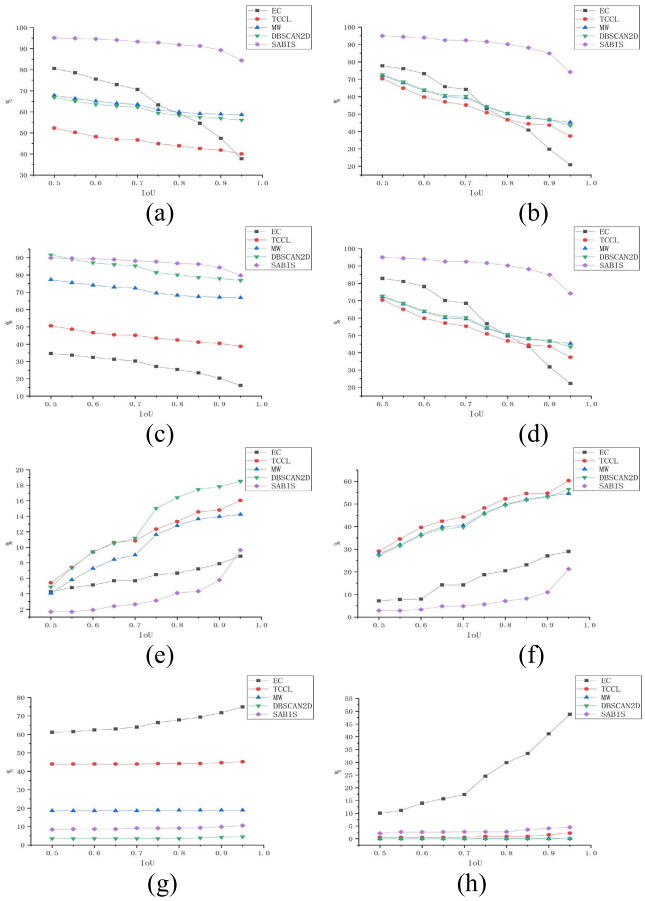

Fig. 21. Five-method segmentation dataset2 accuracy variation curves of the evaluation method based on single object and the evaluation method based on point with the increase of overlap degree. (a) Result of five-method $\boldsymbol{cor_{obj}}$ curve, (b) result of five-method $\boldsymbol{cor_{point}}$ curve, (c) result of five-method $\boldsymbol{com_{obj}}$ curve, (d) result of five-method $\boldsymbol{com_{point}}$ curve, (e) result of five-method $\boldsymbol{und_{obj}}$ curve, (f) result of five-method $\boldsymbol{und_{point}}$ curve, (g) result of five-method $\boldsymbol{over_{obj}}$ curve, and (h) result of five-method $\boldsymbol{over_{point}}$ curve.

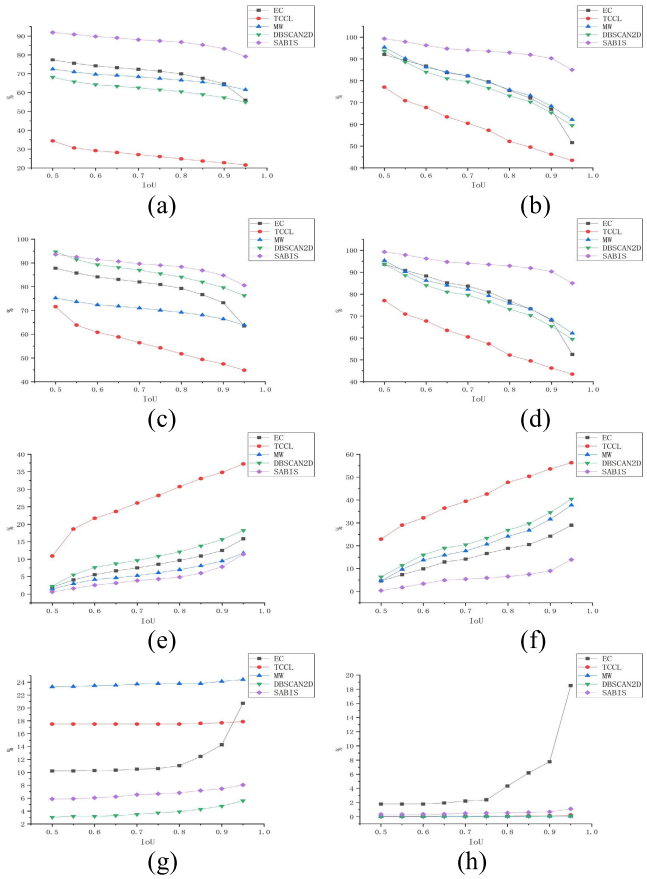

Fig. 22. Five-method segmentation dataset3 accuracy variation curves of the evaluation method based on single object and the evaluation method based on point with the increase of overlap degree. (a) Result of five-method $\boldsymbol{cor_{obj}}$ curve, (b) result of five-method $\boldsymbol{cor_{point}}$ curve, (c) result of five-method $\boldsymbol{com_{obj}}$ curve, (d) result of five-method $\boldsymbol{com_{point}}$ curve. (e) result of five-method $\boldsymbol{und_{obj}}$ curve, (f) result of five-method $\boldsymbol{und_{point}}$ curve, (g) result of five-method $\boldsymbol{over_{obj}}$ curve, and (h) result of five-method $\boldsymbol{over_{point}}$ curve.

segmented individual buildings have lower completeness). The TCCL method tends to have lower completeness of buildings individual segmentation. However, the MW method and the DBSCAN2D method are less affected by the overlap degree, but their overall completeness is lower compared to the proposed method. It can be seen from Figs. 20(b) and (d), 21(b) and (d), and 22(b) and (d) that the EC method is greatly affected by the overlap degree. The TCCL method, the MW method, and the DBSCAN2D method are less affected by the overlap degree, but the values of $\text{cor}_{\text{point}}(\%)$ and $\text{com}_{\text{point}}(\%)$ of these four methods are lower than that of the SABIS method. It can be seen from Figs. 20(a) and (c), 21(a) and (c), and 22(a) and (c) that the EC method and TCCL method are more affected by overlapping images, and $\text{com}_{\text{obj}}(\%)$ decreases rapidly with the increase of overlap degree. The $\text{com}_{\text{obj}}(\%)$ value of the MW method and the DBSCAN2D method is less affected by the overlap degree, but lower than that of the proposed SABIS method. As can be seen from Figs. 20(g) and (h), 21(g) and (h), and 22(g) and (h), the EC method is greatly affected by the overlap degree, and its $\text{over}_{\text{obj}}(\%)$ value and $\text{over}_{\text{point}}(\%)$ value increase rapidly with the increase of overlap degree. As can be seen from Figs. 20(e)–(h), 21(e)–(h), and 22(e)–(h). The values of $\text{und}_{\text{obj}}(\%)$ and $\text{und}_{\text{point}}(\%)$ and $\text{over}_{\text{obj}}(\%)$ and $\text{over}_{\text{point}}(\%)$ of the EC method, the TCCL method, the MW method, and the DBSCAN2D method are basically larger than those of the proposed SABIS method. Furthermore, for each dataset, both the undersegmentation and oversegmentation accuracy based on object and point-based evaluation methods are higher than those achieved by the SABIS method proposed in this article. The ten indicator curves generated by five different building instance segmentation methods on three datasets reveal that the EC method is greatly influenced by the degree of overlap, resulting in a large number of oversegmented individual buildings. The TCCL method, the MW method, and the DBSCAN2D method are less affected by the degree of overlap in terms of accuracy evaluation, but they also produce a significant number of undersegmented individual building. Through the comparative analysis of experimental results on multiple large-scale datasets and the curves depicting the variation of accuracy evaluation results with overlap using multiple evaluation methods, it can be observed that the performance of the proposed SABIS method in this section is significantly better than those of the four currently most classic algorithms.

V. Conclusion

In this article, we propose an SABIS based on large-scale airborne LiDAR point clouds. This method classifies buildings into urban scene buildings and rural residential area buildings by utilizing techniques, such as roof point cloud segmentation, facade point cloud segmentation, object segmentation, feature extraction, and construction of object cylinder neighborhood graphs. Different building individual segmentation methods are used for different types of buildings, enabling SABIS based on large-scale airborne LiDAR point clouds. The feasibility of the proposed SABIS algorithm has been validated by using three large scene datasets at home and abroad. A comparison has been made with four benchmark methods and eight metrics to analyze the robustness of the proposed SABIS algorithm. The proposed algorithm in this article achieves accuracy indicators of over 86% in all aspects, outperforming the existing state-of-the-art algorithms. However, there are certain limitations to the proposed algorithm. For example, in regions with significant variations in point cloud density due to material reflections, some buildings may have missing points or be excessively complex building, leading to instances of oversegmentation or undersegmentation of individual buildings. In future work, we aim to further optimize the algorithm by incorporating additional data sources, such as imagery to enhance the accuracy of building individual segmentation.

Acknowledgment

The authors are grateful to the Dutch for AHN3 (Actueel Hoogtebestand Nederland) dataset.

References

[1] N. Yang, Z. Qin, and Z. Li, "Laser footprint detection and separation method of one single building based on the airborne LiDAR point clouds," *Geomatics Sci. Eng.*, vol. 33, no. 6, p. 4. 2013.

[2] J. Du et al., "A novel framework for 2.5-D building contouring from large-scale residential scenes," *IEEE Trans. Geosci. Remote Sens.*, vol. 57, no. 6, pp. 4121–4145, Jun. 2019.

[3] Y. Zhang, W. Yang, X. Liu, Y. Wan, X. Zhu, and Y. Tan, "Unsupervised building instance segmentation of airborne LiDAR point clouds for parallel reconstruction analysis," *Remote Sens.*, vol. 13, no. 6, p. 1136, Mar. 2021.

[4] W. Yang, X. Liu, Y. Zhang, Y. Wan, and Z. Ji, "Object-based building instance segmentation from airborne LiDAR point clouds," *Int. J. Remote Sens.*, vol. 43, no. 18, pp. 6783–6808, Sep. 2022.

[5] A. Gamal et al., "Automatic LiDAR building segmentation based on DGCNN and Euclidean clustering," *J. Big Data*, vol. 7, p. 102, Nov. 2020.

[6] B. C. Matei et al., "Building segmentation for densely built urban regions using aerial LiDAR data," in *Proc. IEEE Conf. Comput. Vis. Pattern Recognit.*, Jun. 2008, pp. 1–8.

[7] M. Awrangjeb and C. S. Fraser, "Automatic segmentation of raw LiDAR data for extraction of building roofs," *Remote Sens.*, vol. 6, no. 5, pp. 3716–3751, 2014.

[8] R. Cao, Y. Zhang, X. Liu, and Z. Zhao, "3D building roof reconstruction from airborne LiDAR point clouds: A framework based on a spatial database," *Int. J. Geographical Inf. Sci.*, vol. 31, nos. 7–8, pp. 1359–1380, 2017.

[9] F. Tarsha Kurdi and M. Awrangjeb, "Automatic evaluation and improvement of roof segments for modelling missing details using LiDAR data," *Int. J. Remote Sens.*, vol. 41, no. 12, pp. 4702–4725, Jun. 2020.

[10] L. Yan and F. Wei, "Single part of building extraction from dense matching point cloud," *Chin. J. Lasers*, vol. 45, no. 7, 2018, Art. no. 0710004.

[11] J. Gao and R. Yang, "Online building segmentation from ground-based LiDAR data in urban scenes," in *Proc. Int. Conf. 3D Vis. (3DV)*, Jun. 2013, pp. 49–55.

[12] S. Xia and R. Wang, "Façade separation in ground-based LiDAR point clouds based on edges and windows," *IEEE J. Sel. Topics Appl. Earth Observ. Remote Sens.*, vol. 12, no. 3, pp. 1041–1052, Mar. 2019.

[13] X. Wang et al., "A robust segmentation framework for closely packed buildings from airborne LiDAR point clouds," *Int. J. Remote Sens.*, vol. 41, no. 14, pp. 5147–5165, Jul. 2020.

[14] X. Zeng, S. Araki, and K. Kakizaki, "An improved extraction method of individual building wall points from mobile mapping system data," in *Proc. 6th Int. Conf. Innov. Comput. Technol. (INTECH)*, Aug. 2016, pp. 365–370.

[15] S. Ural and J. Shan, "Min-cut based semantic building labeling for airborne LiDAR data," *ISPRS Ann. Photogramm., Remote Sens. Spatial Inf. Sci.*, vol. 5, no. 2, pp. 305–312, Aug. 2020.

[16] M. Awrangjeb and C. S. Fraser, "Rule-based segmentation of LiDAR point cloud for automatic extraction of building roof planes," *ISPRS Ann. Photogramm., Remote Sens. Spatial Inf. Sci.*, vol. 2, pp. 1–6, Oct. 2013.

[17] B. Guo, X. Huang, F. Zhang, and G. Sohn, "Classification of airborne laser scanning data using jointboost," *ISPRS J. Photogramm. Remote Sens.*, vol. 100, pp. 71–83, Feb. 2015.

[18] D. Comaniciu and P. Meer, "Mean shift: A robust approach toward feature space analysis," *IEEE Trans. Pattern Anal. Mach. Intell.*, vol. 24, no. 5, pp. 603–619, May 2002.

[19] X. Huang, R. Cao, and Y. Cao, "A density-based clustering method for the segmentation of individual buildings from filtered airborne LiDAR point clouds," *J. Indian Soc. Remote Sens.*, vol. 47, no. 6, pp. 907–921, Jun. 2019.

[20] Q. Lin, P. Dong, and J. Y. Lin, "A survey on graph cut techniques," *Microprocessors*, vol. 36, no. 1, p. 5, 2015.

[21] Y. Boykov, O. Veksler, and R. Zabih, "A new algorithm for energy minimization with discontinuities," in *Energy Minimization Methods in Computer Vision and Pattern Recognition: Second International Workshop, EMMCVPR'99 York, UK, July 26–29, 1999 Proceedings 2*. Berlin, Germany: Springer, 1999, pp. 205–220.

[22] Y. Boykov, O. Veksler, and R. Zabih, "Fast approximate energy minimization via graph cuts," in *Proc. Int. Conf. Comput. Vis.*, vol. 1, 1999.

[23] Y. Boykov, O. Veksler, and R. Zabih, "Fast approximate energy minimization via graph cuts," *IEEE Trans. Pattern Anal. Mach. Intell.*, vol. 23, no. 11, pp. 1222–1239, Nov. 2001.

[24] V. Kolmogorov, R. Zabih, and S. Gortler, "Generalized multi-camera scene reconstruction using graph cuts," in *Proc. Int. Workshop Energy Minimization Methods Comput. Vis. Pattern Recognit.*, 2003, pp. 501–516.

[25] P. F. Felzenszwalb and D. P. Huttenlocher, "Efficient graph-based image segmentation," *Int. J. Comput. Vis.*, vol. 59, no. 2, pp. 167–181, 2004.

[26] J. Yan, J. Shan, and W. Jiang, "A global optimization approach to roof segmentation from airborne LiDAR point clouds," *ISPRS J. Photogramm. Remote Sens.*, vol. 94, pp. 183–193, Aug. 2014.

[27] Y. Gu, Z. Cao, and L. Dong, "A hierarchical energy minimization method for building roof segmentation from airborne LiDAR data," *Multimedia Tools Appl.*, vol. 76, no. 3, pp. 4197–4210, Feb. 2017.

[28] Z. Hui, Z. Li, P. Cheng, Y. Y. Ziggah, and J. Fan, "Building extraction from airborne LiDAR data based on multi-constraints graph segmentation," *Remote Sens.*, vol. 13, no. 18, p. 3766, Sep. 2021.

[29] S. Du, Z. Zou, Y. Zhang, X. He, and J. Wang, "A building extraction method via graph cuts algorithm by fusion of LiDAR point cloud and orthoimage," *Acta Geodaetica et Cartographica Sinica*, vol. 47, no. 4, p. 519, 2018.

Wangshan Yang received the Ph.D. degree in photogrammetry and remote sensing from the School of Remote Sensing and Information Engineering, Wuhan University, Wuhan, China, in 2022.

He is currently a Lecturer with China Jiliang University, Hangzhou, China. His research interests include point cloud processing, 3-D reconstruction, and computer vision.

Yongjun Zhang (Member, IEEE) received the B.S. degree in geodesy, the M.S. degree in geodesy and surveying engineering, and the Ph.D. degree in geodesy and photography from Wuhan University, Wuhan, China, in 1997, 2000, and 2002, respectively.

He is currently a Dean of the School of Remote Sensing and Information Engineering, Wuhan University, where he has been a Full Professor with the School of Remote Sensing and Information Engineering since 2006. He has authored or co-authored more than 150 research articles and one book. He holds 25 Chinese patents and 26 copyright-registered computer software. His research interests include aerospace and low-attitude photogrammetry, image matching, combined block adjustment with multisource datasets, object information extraction and modeling with artificial intelligence, integration of LiDAR point clouds and images, and 3-D city model reconstruction.

Xinyi Liu received the B.S. and Ph.D. degrees in photogrammetry and remote sensing from the School of Remote Sensing and Information Engineering, Wuhan University, Wuhan, China, in 2014 and 2020, respectively.

She currently holds a post-doctoral position with Wuhan University. Her research interests include 3-D reconstruction, LiDAR and image integration, and texture mapping.

Boyong Gao received the B.S. degree in forging from the Northeast Heavy Machinery Institute, Qiqihaer, China, in 1994, the M.S. degree in metal plastic processing from the Huazhong University of Science and Technology, Wuhan, China in 1997, and the Ph.D. degree in computer science and technology from Zhejiang University, Hangzhou, China, in 2011.

He is currently an Associate Professor with the College of Information Engineering, China Jiliang University, Hangzhou. His research interests include machine learning in time series and multimedia analysis.